Polymer-Supported Liquid Layer Electrolyzer Enabled Electrochemical CO_2 Reduction to CO with High Energy Efficiency

Shangyu Li,[a] Yiwen Ma,[a] Tiancheng Zhao,[a] Jiaxin Li,[a] Xinyue Kang,[a] Wen Guo,[a] Yunzhou Wen,[a] Liping Wang,[a] Yurui Wang,[b] Renxing Lin,[b] Tiantian Li,[b] Hairen Tan,*[b] Huisheng Peng,*[a] and Bo Zhang*[a]

The electrochemical conversion of carbon dioxide (CO_2) to carbon monoxide (CO) is a favorable approach to reduce CO_2 emission while converting excess sustainable energy to important chemical feedstocks. At high current density ($>100\ mA\,cm^{-2}$), low energy efficiency (EE) and unaffordable cell cost limit the industrial application of conventional CO_2 electrolyzers. Thus, a crucial and urgent task is to design a new type of CO_2 electrolyzer that can work efficiently at high current density. Here we report a polymer-supported liquid layer (PSL) electrolyzer using polypropylene non-woven fabric as a separator between anode and cathode. Ag based cathode was fed with humid CO_2 and potassium hydroxide was fed to earth-abundant NiFe-based anode. In this configuration, the PSL provided high-pH condition for the cathode reaction and reduced the cell resistance, achieving a high full cell EE over 66% at $100\ mA\,cm^{-2}$.

1. Introduction

In recent decades, the atmospheric CO_2 concentration has been rising rapidly from 290 to 400 ppm, leading to a series of environmental issues.[1] The development of cost efficiency CO_2 utilization technologies to reduce CO_2 levels and reconciling carbon-cycle is of great importance.[2] Electrochemical CO_2 reduction (eCO_2R) using sustainable energy to formic acid,[3] carbon monoxide (CO),[4] methanol,[5] ethanol,[6] ethylene,[7] etc., could provide a new approach for utilizing the excess CO_2. CO is a versatile feedstock which can be facilely converted to high-value oxygenates and hydrocarbons through the Fischer-Tropsch process.[8] Techno-economic assessment has shown that CO production via eCO_2R method can be potentially achieved competitively against conventional fossil-fuel based processes.[9]

The levelized cost of eCO_2R to CO contains capital investment like electrolyzer cost and operational costs such as CO_2 feedstock, electricity consumption, and product separation.[10] Among them, the electricity consumption is one of the major costs and is mainly affected by the EE of the CO_2 electrolyzer, which is also a decisive factor to limit the development of efficient eCO_2R towards industrialization. EE depends on the full cell voltage and CO Faradaic efficiency (COFE):

$$EE = \frac{E_0 * COFE}{V}$$

where E_0 is the thermodynamic equilibrium potential of the total reaction, and V represents the cell voltage. eCO_2R to CO is a pH-dependent reaction,[11] and the increase of hydroxide concentration will promote CO_2 to CO reaction and suppress hydrogen evolution reaction (HER). Hence, high pH condition is a crucial goal for the design of eCO_2R-to-CO electrolyzer.

To date, two main architectures including gas-phase and liquid-phase electrolyzers have been reported for eCO_2R to CO. Gas-phase electrolyzers use polymer electrolyte membranes (PEM) such as cation exchange membrane (CEM),[12] anion exchange membrane (AEM)[13] or bipolar membrane (BPM)[14] between cathode and anode (Figure 1a). For the membrane electrolyte, it is difficult to provide high pH conditions for the cathode, so COFE in electrolyzers with CEM or BPM is still much lower than 90% when current density exceeds $100\ mA\,cm^{-2}$.[8,12,14–15] The usage of AEM can make an improvement of the COFE compared with the former two membranes, but the high cell voltage still results in low EE and cannot meet the industrial requirements.[13,16]

While, in liquid-phase electrolyzers,[17] a high pH environment at the cathode can be easily achieved by tuning the pH of the liquid electrolyte, which can promote the eCO_2R to CO process (Figure 1b). Moreover, the alkaline condition of liquid-

[a] S. Li, Y. Ma, T. Zhao, J. Li, X. Kang, W. Guo, Y. Wen, L. Wang, Prof. H. Peng, Prof. B. Zhang
State Key Laboratory of Molecular Engineering of Polymers
Department of Macromolecular Science and Laboratory of Advanced Materials, Fudan University
200438 Shanghai (P. R. China)
E-mail: penghs@fudan.edu.cn
bozhang@fudan.edu.cn
[b] Y. Wang, R. Lin, T. Li, Prof. H. Tan
National Laboratory of Solid State Microstructures
Jiangsu Key Laboratory of Artificial Functional Materials
College of Engineering and Applied Science, Nanjing University
210093 Jiangsu (P. R. China)
E-mail: hairentan@nju.edu.cn

Supporting information for this article is available on the WWW under https://doi.org/10.1002/open.202100084

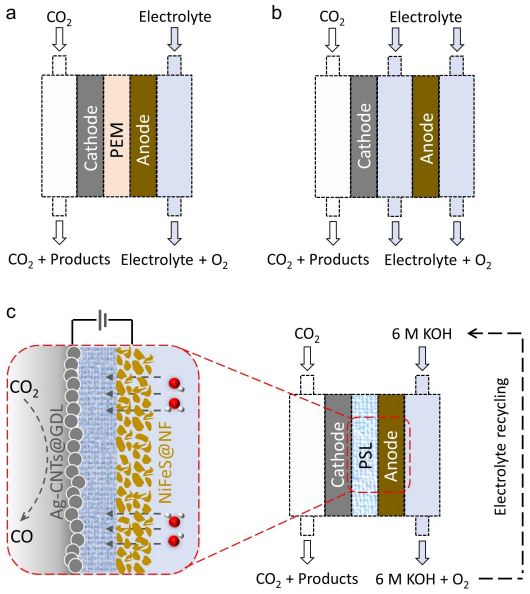

Figure 1. a) Gas-phase electrolyzer with polymer electrolyte membranes (PEM). b) Liquid-phase electrolyzer. c) Polymer-supported liquid layer (PSL) electrolyzer.

phase electrolyzers can avoid the usage of noble iridium oxide catalysts at the anode, which can decrease the capital cost of the electrolyzer. However, the electrolyte layer in the liquid-phase electrolyzer structure usually brings considerable ohmic loss, resulting in the increase of cell voltage and EE.[16b]

Herein, we report a polymer-supported liquid layer (PSL) electrolyzer for eCO_2R to CO, which uses a polypropylene non-woven fabric separating the anode and cathode to avoid short circuit and also maintain liquid electrolyte in it (Figure 1c). The anolyte continuously passes through the anode and wets the fabric to provide a high-pH condition for the cathode. In this configuration, we achieved a low ohmic resistance and reduced the voltage fluctuations commonly seen in liquid-phase electrolyzers.[16b,18] As a result, the PSL electrolyzer delivered a near unity CO selectivity with only 0.2% H_2 FE, a low cell voltage of 2 V, and a high EE of 66% at a current density of 100 mA cm^{-2}.

2. Results and Discussion

2.1. Design of Electrolyzer Architecture and Catalyst Characterization

We designed a membrane-free liquid-phase electrolyzer, which comprised a series of polymethyl methacrylate plates and silicone pads between the cathode and anode (Figure 1b and Figure S1 in the Supporting Information). Ag nanoparticles (AgNPs) and homemade multi-walled carbon nanotubes (MWCNTs)[19] were mixed and deposited onto the carbon gas diffusion layer to produce the Ag-based cathode (Figure S2a in the Supporting Information). Scanning electron micrographs (SEM) revealed a homogeneous mixture of AgNPs and MWCNTs at the top of the carbon gas diffusion layer (Figure S3 in the Supporting Information). In addition, high resolution transmission electron micrographs (TEM) revealed that nanoparticles exhibited a similar size around 30 nm (Figure S4 in the Supporting Information). The X-ray photoelectron spectroscopy (XPS) and the X-ray diffraction (XRD) patterns of the cathode showed a metallic phase of Ag catalyst (Figure S5 in the Supporting Information). In order to reduce the cost, a nickel foam loaded with Fe-doped Ni_3S_2 arrays (NiFeS@NF) catalysts was used as the anode, which was prepared through a one-pot hydrothermal method[20] (Figure S2b in the Supporting Information). The geometric active areas of the anode and cathode were both 1 cm^2. The cathode was fed with a humid CO_2 gas stream, and the anode was fed with 6 M KOH by a peristaltic pump.

2.2. Effect of Electrolyte Layer Thickness on Enhancing EE

To study the influence of the liquid electrolyte layer thickness on COFE and EE, different polymethyl methacrylate plates and silicone pads were used to obtain liquid-phase electrolyzers with various thicknesses of electrolyte layers. These cells were operated at identical current density of 100 mA cm^{-2}. As shown in Figures 2a–2c, when the thickness of middle liquid layer was reduced from 10 to 1 mm, the cell voltage decreased from 2.39 to 2.12 V. Whereas the COFE was almost stable at around 100%, and there was an increase of the EE from 55% to 62% (Figure 2e). Ohmic resistance of the cell was measured using electrochemical impedance spectroscopy method. The potentiostatic mode was used at a cell voltage of 1.6 V (Figure S6 in the Supporting Information). With the electrolyte layer thickness of 10 mm, 4 mm, and 1 mm, the cell resistance was 3.38 Ω cm^{-2}, 2.63 Ω cm^{-2}, 1.74 Ω cm^{-2}, respectively (Figure 2e). The reduction of the electrolyte thickness resulted in a 40% decline in the energy wastage due to the ohmic loss (Figure S7 in the Supporting Information). Theoretically, the cell resistance can continue to decrease as the thickness of the liquid layer declines, further improving the EE. However, in the real cell assembly process, when the electrolyte layer becomes thinner, the anode and cathode often contact with each other, resulting in short circuit and device failure.

To solve the above problem, we used a piece of polypropylene non-woven fabric absorbing liquid electrolyte as the PSL to better separate the anode and cathode and produced a liquid layer thickness of 0.6 mm. The structure information and parameters were shown in Figure S8 and Table S1. The fabric wetted with 6 M KOH electrolyte provided a high pH condition for the cathode. As shown in Figures 2d and 2e, the usage of PSL further reduced the cell resistance to 1.15 Ω cm^{-2}, and the cell voltage at 100 mA cm^{-2} accordingly dropped to 2 V. The full cell EE of the PSL architecture surpassed 66% at 100 mA cm^{-2}, saving 20% electricity compared with traditional 10-mm-layer liquid-phase electrolyzer. In comparison with the liquid-phase electrolyzer, this configuration has a more stable voltage, avoiding the voltage fluctuation that often occurs in traditional liquid-phase electrolyzer config-

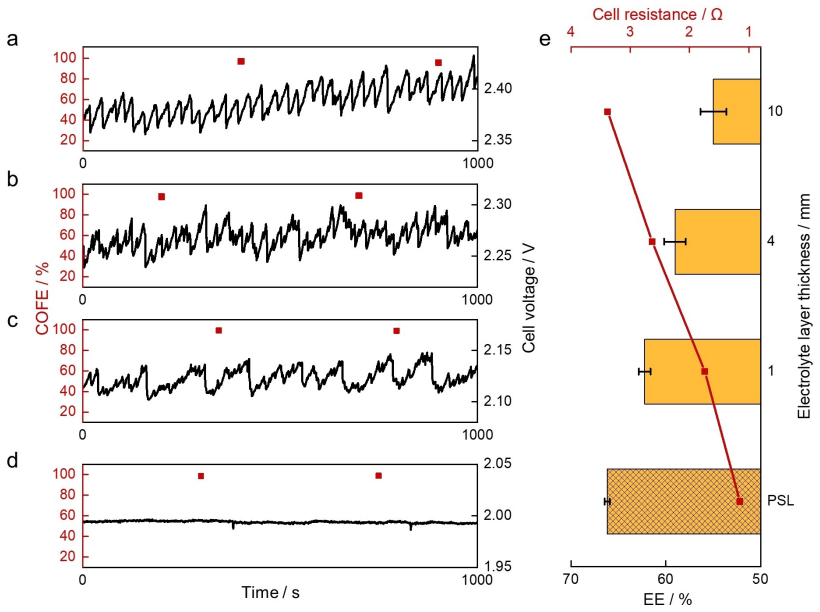

Figure 2. a–d) COFE and cell voltage of liquid-phase electrolyzers with 10-, 4-, and 1-mm electrolyte thickness and PSL at 100 mA cm^{-2}. e) Cell resistance and EE of liquid-phase electrolyzers with 10-, 4-, and 1-mm electrolyte thickness and PSL.

uration. The reason for the weakness of voltage fluctuation could be ascribed to the restriction of oxygen diffusion to the middle electrolyte layer by a zero-gap structure.[21]

2.3. Cell Performance

As revealed in Figure 3a, the cell voltage of the PSL electrolyzer was only 1.62 V at 10 mA cm^{-2}. Even at such a low voltage, COFE was still over 98%, indicating that the high pH environment provided by the liquid layer effectively inhibited HER, thus providing the energy conversion efficiency of full cell to be up to 80%. The cell voltage increased continuously with the current density, whereas COFE remained greater than 98% when the current density increased to 100 mA cm^{-2}, and H_2FE eventually fell to only 0.2% (Figure S9 in the Supporting Information). To further assess the current/voltage characteristics of our PSL electrolyzer, the linear sweep voltammogram (LSV) was scanned at 10 mV s^{-1} within the cell voltage range from 1.2 to 2.4 V (Figure S10 in the Supporting Information). When the cell voltage is above 2.0 V, the I–V curve appeared to be linear, indicating that the I–V response was not limited by the reaction rates of anode and cathode, but dominated by the ohmic resistance of the electrolyzer. The above results positively indicated that the PSL electrolyzer has the potential for efficient eCO_2R to CO at a high current density.

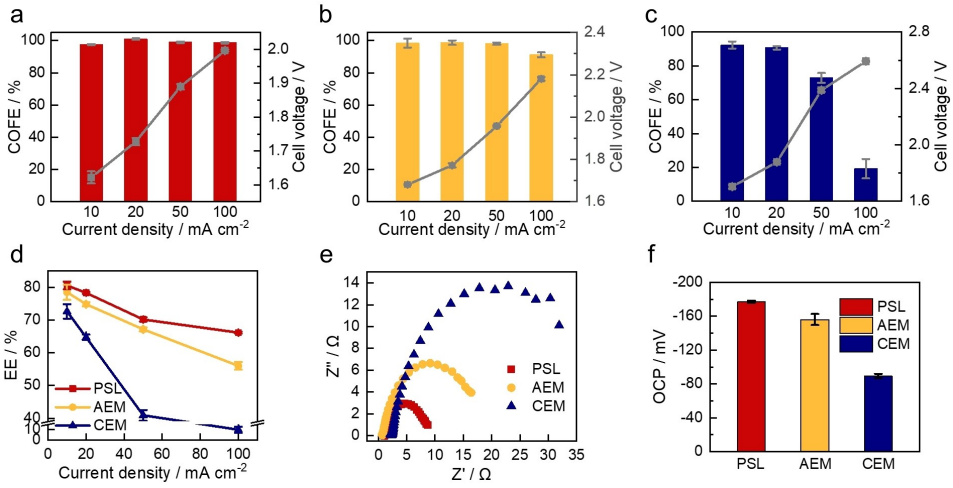

Figure 3. (a–c) COFE and cell voltage at current densities between 10 to 100 mA cm^{-2} of PSL, AEM and CEM electrolyzers, respectively. d) Full cell energy efficiency of PSL, AEM and CEM electrolyzers. e) Nyquist diagram at a constant cell voltage of 1.6 V. f) Relative pH comparison of three electrolyzers using an open circuit potential (OCP) measurement.

To compare with the gas-phase electrolyzers using AEM and CEM membranes, we replaced the polypropylene non-woven fabric by commercial Sustanion AEM and Nafion-117 CEM, respectively, using the same assembly method. As shown in Figure 3b, the cell voltage of the AEM electrolyzer was higher than that of the PSL electrolyzer at all current densities. The COFE was maintained at about 98% at low current density, but when the current density reached 100 mA cm^{-2}, the COFE dropped to 90%. The cell voltage of CEM was much higher than the PSL and AEM cells, and the COFE sharply dropped below 75% and 20% at 50 and 100 mA cm^{-2}, respectively (Figure 3c and S11 in the Supporting Information). One reason for the low COFE of the CEM cell is that only H^+ and K^+ ions can diffuse across the membrane, which cannot provide enough high pH environment for the cathode. Therefore, with the increase of current densities, HER replaced eCO_2R and became the dominant cathodic reaction.

The full cell EE of the three configurations for eCO_2R to CO was shown in Figure 3d, in which the PSL cell exhibited much greater EE than the other two cells. To understand the difference between the PSL, AEM, and CEM electrolyzers, electrochemical impedance spectroscopy was measured at a constant cell voltage of 1.6 V. The ohmic resistance of the PSL electrolyzer was close to the AEM electrolyzer and much lower than the CEM electrolyzer, but this affected the selectivity of CO little and was not the main reason for the difference of the cell performance. The charge transfer resistance of the PSL electrolyzer was 2.3 and 5 times lower than that of the AEM and CEM electrolyzers, respectively (Figure 3e). Because the three cells had the same anode and cathode configurations, the improvement of the cell performance could be attributed to the enhanced charge transfer at the interface between cathode and electrolyte. Since eCO_2R to CO is a pH-dependent reaction, the hydroxyl ion concentration could account for the difference of charge transfer resistance among the three cells. To verify this explanation, we compared the relative pH values of the three cathode/electrolyte interfaces using a similar method reported in the previous works.[22] The open-circuit potential is linearly related to pH value, and the more negative the open-circuit potential, the higher the pH of the solution. As shown in Figure 3f, the PSL electrolyzer had the most negative open-circuit potential with the highest pH value at the cathode/electrolyte interface among the three configurations. We further conducted Tafel polarization measurements in different electrolyzers. As shown in Figure S12, the slopes were measured to be 215 mV dec^{-1}, 187 mV dec^{-1}, and 152 mV dec^{-1}, for CEM, AEM, and PSL electrolyzers, respectively. The lowest Tafel slope value of 152 mV dec^{-1} also suggested that a higher pH condition for the cathode in PSL structure, which facilitated the eCO_2R reaction.[11]

Since the formation of bicarbonate/carbonate is an issue for conducting eCO_2R in alkaline electrolyzers, we investigated the stability of our PSL electrolyzer and monitored the pH value of the anolyte (Figure S13 in the Supporting Information). The PSL electrolyzer operated at a current density of 50 mA cm^{-2} for two hours, with a stable high COFE (> 90%) and slightly increases of the cell voltage (< 4%). The pH value of the anolyte remained almost constant, and no carbonate precipitate was observed on the microporous layer of the GDL.

2.4. Solar-Driven CO_2-to-CO System

To further fully take advantage of the high EE and low cell voltage, we coupled the PSL electrolyzer with a 24.3%-efficiency all-perovskite monolithic tandem photovoltaic cell (Figure S14 in the Supporting Information) to compose a solar-driven CO_2-to-CO system. The tandem cells were fabricated according to previous works,[23] and powered by simulated AM 1.5G irradiation.

The electrolyzer and the tandem cell have identical areas of 1 cm^2. The solar-to-CO efficiency of this system can be calculated as follows:

$$\text{Solar-to-CO efficiency} = \frac{E_0 * I * COFE}{P_{solar}}$$

where I is the current density of the system, and P_{solar} represents the power density of AM 1.5G irradiation (100 mW cm^{-2}). The current density of the system can be estimated by the intersection of the individual I–V curves of the tandem cell and the PSL electrolyzer, i.e. ~14.6 mA cm^{-2} at 1.68 V (Figure 4a). Due to high COFE (> 98%) of our PSL electrolyzer, we can achieve a high solar-to-CO efficiency over 19% at the intersection. When the PV connected to the PSL electrolyzer at steady-state mode under simulated AM 1.5G irradiation, the PSL-PV standalone system showed a stabilized solar-to-CO efficiency of 14.3% (Figure 4b). The loss between the steady-state efficiency and the intersection efficiency may be due to the increase of system ohmic resistance during the actual connection.

3. Conclusion

In summary, we report a configuration of the eCO_2R to CO electrolyzer with a polypropylene non-woven fabric to separate the anode and cathode. The fabric wetted by the electrolyte forms a thin PSL with only a 0.6-mm-thickness. When a strong alkaline electrolyte is used, this configuration provides a high pH condition for the cathode and achieves an ultra-low cell resistance, avoiding the disadvantages of conventional gas-phase and liquid-phase electrolyzers. Only using relatively low-cost catalysts like Ag as the cathode and NiFeS as the anode, the EE of the PSL cell is up to 80% and 66% under the operating condition of 10 and 100 mA cm^{-2}, respectively, with the COFE remaining above 98%. Compared to the conventional gas-phase and liquid-phase electrolyzers, the PSL cell showed the highest EE reported in the literature (Table 1).

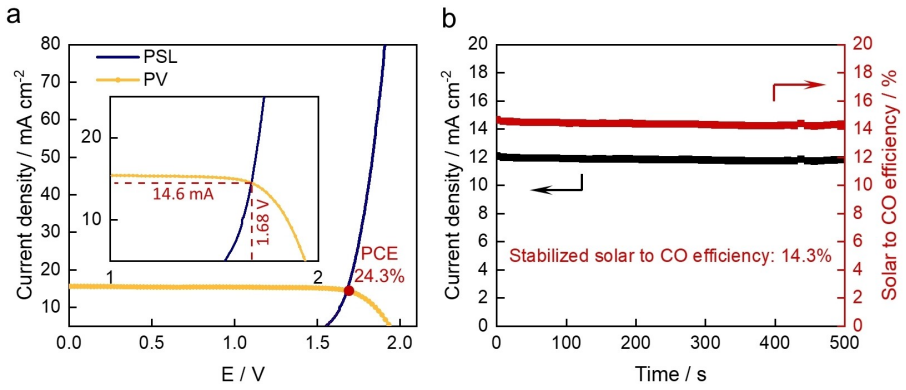

Figure 4. a) *I–V* curves of the all-perovskite tandem solar cell under simulated AM 1.5G 1 Sun solar irradiation and the PSL electrolyzer (PCE, power conversion efficiency). b) Solar-to-CO efficiency and current density of the solar-driven CO_2-to-CO system. The active areas of the PV cell and the PSL electrolyzer are both 1 cm^2.

Table 1. Summary of reported eCO_2R to CO electrolyzers.

Configuration	Current density [mA cm^{-2}]	EE [%]	Cell voltage [V]	COFE [%]	Ref.
PSL	**100**	**66.2**	**2.0**	**98.7**	**This work**
Liquid-phase electrolyzer	100	60	/	/	[17]
	350	45	3	95	
Liquid-phase electrolyzer	417	53	2.5	100	[24]
Liquid-phase electrolyzer	100	~43	2.8	~90	[16b]
AEM	100	~43	3.0	96.9	[13]
AEM[a]	100	~57	2.25	~95	[16b]
AEM[a]	630	40	3.2	~85	[25]
CEM	50	~43	2.8	~90	[12]
BPM	100	~25	~3.5	65.0	[8]

[a] Electrolysis at 60 °C.

Acknowledgements

This work was supported by NSFC (21875042, 21634003, 51573027), MOST (2016YFA0203302), and STCSM (18QA140080, 16JC1400702). This work was also supported by the Program for Eastern Scholars at Shanghai Institutions. The work of H. T. was supported by the National Natural Science Foundation of China (61974063).

Conflict of Interest

The authors declare no conflict of interest.

Keywords: CO_2 conversion · electrochemical reduction · electrolyzers · polymer-supported liquid layers · low cell voltage

[1] K. Hashimoto, in *Global Carbon Dioxide Recycling: For Global Sustainable Development by Renewable Energy*, Springer Singapore, Singapore, **2019**, pp. 5–17.
[2] a) Y. Y. Birdja, E. Pérez-Gallent, M. C. Figueiredo, A. J. Göttle, F. Calle-Vallejo, M. T. M. Koper, *Nat. Energy* **2019**, *4*, 732–745; b) P. De Luna, C. Hahn, D. Higgins, S. A. Jaffer, T. F. Jaramillo, E. H. Sargent, *Science* **2019**, *364*, eaav3506.
[3] S. He, F. Ni, Y. Ji, L. Wang, Y. Wen, H. Bai, G. Liu, Y. Zhang, Y. Li, B. Zhang, H. Peng, *Angew. Chem. Int. Ed.* **2018**, *57*, 16114–16119; *Angew. Chem.* **2018**, *130*, 16346–16351.
[4] S. Ren, D. Joulié, D. Salvatore, K. Torbensen, M. Wang, M. Robert, C. P. Berlinguette, *Science* **2019**, *365*, 367–369.
[5] W. Zhang, Q. Qin, L. Dai, R. Qin, X. Zhao, X. Chen, D. Ou, J. Chen, T. T. Chuong, B. Wu, N. Zheng, *Angew. Chem. Int. Ed.* **2018**, *57*, 9475–9479; *Angew. Chem.* **2018**, *130*, 9619–9623.
[6] Y. Liu, Y. Zhang, K. Cheng, X. Quan, X. Fan, Y. Su, S. Chen, H. Zhao, Y. Zhang, H. Yu, M. R. Hoffmann, *Angew. Chem. Int. Ed.* **2017**, *56*, 15607–15611; *Angew. Chem.* **2017**, *129*, 15813–15817.
[7] H. Bai, T. Cheng, S. Li, Z. Zhou, H. Yang, J. Li, M. Xie, J. Ye, Y. Ji, Y. Li, Z. Zhou, S. Sun, B. Zhang, H. Peng, *Sci. Bull.* **2021**, *66*, 62–68.
[8] D. A. Salvatore, D. M. Weekes, J. He, K. E. Dettelbach, Y. C. Li, T. E. Mallouk, C. P. Berlinguette, *ACS Energy Lett.* **2017**, *3*, 149–154.
[9] M. Jouny, W. Luc, F. Jiao, *Ind. Eng. Chem. Res.* **2018**, *57*, 2165–2177.
[10] M. G. Kibria, J. P. Edwards, C. M. Gabardo, C. T. Dinh, A. Seifitokaldani, D. Sinton, E. H. Sargent, *Adv. Mater.* **2019**, *31*, e1807166.
[11] C. M. Gabardo, A. Seifitokaldani, J. P. Edwards, C.-T. Dinh, T. Burdyny, M. G. Kibria, C. P. O'Brien, E. H. Sargent, D. Sinton, *Energy Environ. Sci.* **2018**, *11*, 2531–2539.
[12] S. Jin, Y. Ni, Z. Hao, K. Zhang, Y. Lu, Z. Yan, Y. Wei, Y. R. Lu, T. S. Chan, J. Chen, *Angew. Chem. Int. Ed.* **2020**, *59*, 21885–21889; *Angew. Chem.* **2020**, *132*, 22069–22073.
[13] R. B. Kutz, Q. Chen, H. Yang, S. D. Sajjad, Z. Liu, I. R. Masel, *Energy Technol.* **2017**, *5*, 929–936.
[14] Z. Yan, J. L. Hitt, Z. Zeng, M. A. Hickner, T. E. Mallouk, *Nat. Chem.* **2021**, *13*, 33–40.
[15] E. J. Dufek, T. E. Lister, S. G. Stone, M. E. McIlwain, *J. Electrochem. Soc.* **2012**, *159*, F514–F517.
[16] a) Y. Hori, H. Ito, K. Okano, K. Nagasu, S. Sato, *Electrochim. Acta* **2003**, *48*, 2651–2657; b) Z. Yin, H. Peng, X. Wei, H. Zhou, J. Gong, M. Huai, L. Xiao, G. Wang, J. Lu, L. Zhuang, *Energy Environ. Sci.* **2019**, *12*, 2455–2462.

[17] S. Ma, R. Luo, J. I. Gold, A. Z. Yu, B. Kim, P. J. A. Kenis, *J. Mater. Chem. A* **2016**, *4*, 8573–8578.
[18] S. Verma, Y. Hamasaki, C. Kim, W. Huang, S. Lu, H.-R. M. Jhong, A. A. Gewirth, T. Fujigaya, N. Nakashima, P. J. A. Kenis, *ACS Energy Lett.* **2017**, *3*, 193–198.
[19] L. Ye, M. Liao, T. Zhao, H. Sun, Y. Zhao, X. Sun, B. Wang, H. Peng, *Angew. Chem. Int. Ed.* **2019**, *58*, 17054–17060; *Angew. Chem.* **2019**, *131*, 17210–17216.
[20] B. Fei, Z. Chen, J. Liu, H. Xu, X. Yan, H. Qing, M. Chen, R. Wu, *Adv. Energy Mater.* **2020**, *10*, 2001963.
[21] J.-H. Guo, W.-Y. Sun, *Appl. Catal. B* **2020**, *275*, 119154.
[22] a) Y. Wen, X. Wang, P. Cai, X. Yu, *Sens. Actuators B* **2015**, *216*, 409–411; b) S. Licht, *Anal. Chem.* **1985**, *57*, 514–519.
[23] a) K. Xiao, R. Lin, Q. Han, Y. Hou, Z. Qin, H. T. Nguyen, J. Wen, M. Wei, V. Yeddu, M. I. Saidaminov, Y. Gao, X. Luo, Y. Wang, H. Gao, C. Zhang, J. Xu, J. Zhu, E. H. Sargent, H. Tan, *Nat. Energy* **2020**, *5*, 870–880; b) R. Lin, K. Xiao, Z. Qin, Q. Han, C. Zhang, M. Wei, M. I. Saidaminov, Y. Gao, J. Xu, M. Xiao, A. Li, J. Zhu, E. H. Sargent, H. Tan, *Nat. Energy* **2019**, *4*, 864–873.
[24] S. S. Bhargava, F. Proietto, D. Azmoodeh, E. R. Cofell, D. A. Henckel, S. Verma, C. J. Brooks, A. A. Gewirth, P. J. A. Kenis, *ChemElectroChem* **2020**, *7*, 2001–2011.
[25] B. Endrődi, E. Kecsenovity, A. Samu, T. Halmágyi, S. Rojas-Carbonell, L. Wang, Y. Yan, C. Janáky, *Energy Environ. Sci.* **2020**, *13*, 4098–4105.

Manuscript received: April 7, 2021
Revised manuscript received: April 22, 2021